



# Engineering composition-tunable 3D hierarchical bismuth oxyiodides heterojunctions: Ionic liquid-assisted fabrication with strong adsorption ability and enhanced photocatalytic properties



Meng Sun<sup>a</sup>, Qingquan Wei<sup>a</sup>, Yu Shao<sup>b</sup>, Bin Du<sup>a,c,\*</sup>, Tao Yan<sup>a</sup>, Liangguo Yan<sup>a</sup>, Danzhen Li<sup>b,\*\*</sup>

<sup>a</sup> School of Resources and Environment, University of Jinan, Jinan 250022, PR China

<sup>b</sup> State Key Laboratory of Photocatalysis on Energy and Environment, Research Institute of Photocatalysis, Fuzhou University, Fuzhou 350016, PR China

<sup>c</sup> Key Laboratory of Chemical Sensing & Analysis in Universities of Shandong, School of Chemistry and Chemical Engineering, University of Jinan, Jinan 250022, PR China

## ARTICLE INFO

### Keywords:

Photocatalyst  
Bismuth oxyiodide hybrids  
Phenolic pollutants  
Degradation  
Visible light

## ABSTRACT

In this work, we report the fabrication of composition-tunable heterostructured bismuth oxyiodides photocatalysts using a facile ionic liquid-assisted precipitation method at room temperature. Through elaborately governing the reaction parameters, two groups of bismuth oxyiodide hybrids (Group 1: BiOI/Bi<sub>4</sub>O<sub>5</sub>I<sub>2</sub>, and Group 2: Bi<sub>4</sub>O<sub>5</sub>I<sub>2</sub>/Bi<sub>5</sub>O<sub>7</sub>I) with different components were prepared. The DRS spectra shows that the absorption edges of the hybrids were gradually tuned from 550 to 660 nm, which was in accordance with the color gradient from light yellow (Bi<sub>5</sub>O<sub>7</sub>I) to brick red (BiOI). The SEM images show that the products mainly exhibited 3D hierarchical architecture, which was beneficial for the adsorption of contaminants over the catalyst's surface. The two groups of heterojunction photocatalysts all exhibited remarkably improved photocatalytic activity in decomposing *o*-phenylphenol (OPP) and 4-*tert*-butylphenol (PTBP) under visible light irradiation respect to single phase photocatalyst (BiOI, Bi<sub>4</sub>O<sub>5</sub>I<sub>2</sub>, or Bi<sub>5</sub>O<sub>7</sub>I). For BiOI/Bi<sub>4</sub>O<sub>5</sub>I<sub>2</sub> hybrids, the S5 sample exhibited the optimal activity, which was approximately 5.35 and 1.85 times higher than that of pristine BiOI and Bi<sub>4</sub>O<sub>5</sub>I<sub>2</sub>, respectively. For the second group of Bi<sub>4</sub>O<sub>5</sub>I<sub>2</sub>/Bi<sub>5</sub>O<sub>7</sub>I, the optimal activity was observed for S9 hybrid, which was approximately 2.43 and 2.12 times higher than that of bare Bi<sub>4</sub>O<sub>5</sub>I<sub>2</sub> and Bi<sub>5</sub>O<sub>7</sub>I under identical conditions. This activity enhancement should be attributed to the balanced band levels of the components, which facilitates the fast interfacial charge transmigration of photo-generated carriers, resulting in highly promoted charge separation efficiency. This deduction was proved by the photocurrent, electrochemical impedance spectroscopy, and photoluminescence measurements. The possible degradation mechanisms for BiOI/Bi<sub>4</sub>O<sub>5</sub>I<sub>2</sub> and Bi<sub>4</sub>O<sub>5</sub>I<sub>2</sub>/Bi<sub>5</sub>O<sub>7</sub>I hybrids were proposed based on the band potentials and trapping experiment results.

## 1. Introduction

The environment deterioration is becoming more and more serious all over the world, especially for the developing countries that are rapidly propelling the industrialization and urbanization. Water pollution is one of the prominent problems for environment deterioration. The wastewater discharged from pharmaceutical or biochemical factories, chemical plants, hospitals, and oil refineries all contains phenolic compounds, which are high toxic but with poor biodegradability [1–4]. Phenolic compounds have been considered as top priority pollutants because of their mutagenic and carcinogenic properties [5–7]. Consequently, removing these compounds from wastewater will make great sense to protect the environment and public health [8,9]. Many

traditional methods such as microbial degradation [10], extraction [11,12], adsorption [13,14], and membrane separation [15] have been used to treat phenolic compounds-containing wastewater. However, these conventional techniques were usually slow or inefficient, and sometimes a secondary pollution was unavoidable because of the incomplete removal of contaminants or chemical reagents addition during treatment. On the contrary, the burgeoning photocatalysis technology has been proved to be an efficient method for eliminating hazardous compounds in wastewater [16–19]. Especially for the visible light-responsive photocatalysis, it not only met people's demand of energy-/cost-saving, but also worked under mild reaction conditions without secondary pollution.

In recent years, the bismuth-based oxyhalides have exhibited great

\* Corresponding author at: School of Resources and Environment, University of Jinan, Jinan 250022, PR China.

\*\* Corresponding author.

E-mail addresses: [dubin61@gmail.com](mailto:dubin61@gmail.com) (B. Du), [dzli@fzu.edu.cn](mailto:dzli@fzu.edu.cn) (D. Li).



Fig. 1. Schematic flowchart for the fabrication of composition-tunable 3D hierarchical bismuth oxyiodides heterojunctions.

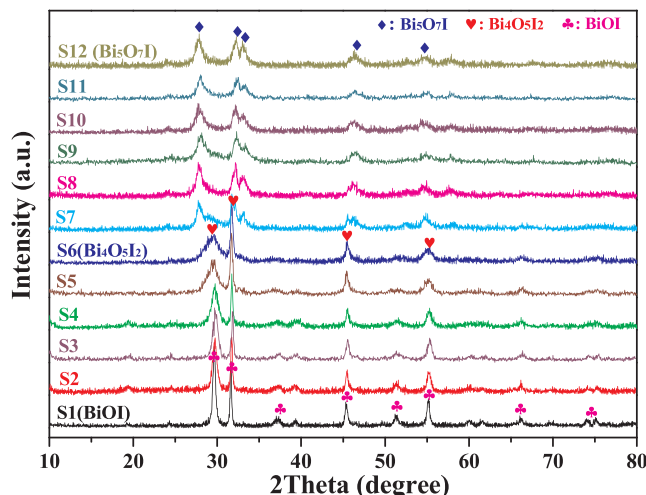


Fig. 2. XRD patterns of as-synthesized two groups of bismuth oxyiodide hybrids.

promise in the photocatalytic degradation of organic contaminants [20–22]. For these materials with layered structure, their internal static electric field would facilitate the transfer and separation of photo-generated charge carriers, as well as promote the photocatalytic performances [23]. For example, Xia and co-workers reported the fabrication of layered  $\text{Bi}_4\text{O}_5\text{I}_2$  photocatalyst with enhanced performances [24]. Zheng et al. prepared  $\text{Bi}_4\text{O}_5\text{Br}_2$  nanoflakes with selective photocatalytic oxidation activity under blue LED irradiation [25].  $\text{Bi}_5\text{O}_7\text{I}$  has also been reported as a novel visible-light responsive photocatalyst by Wu and co-workers [26]. Besides,  $\text{Bi}_7\text{O}_9\text{I}_3$  [27],  $\text{Bi}_{12}\text{O}_{17}\text{Cl}_2$  [28,29],  $\text{Bi}_{24}\text{O}_{31}\text{Cl}_{10}$  [30],  $\text{Bi}_{24}\text{O}_{31}\text{Br}_{10}$  [31], and  $\text{BiOBr}$  [32] all have been reported as visible light responsive photocatalysts. However, the high recombination of charge carries for these single-phase materials severely hindered their practical applications. To surmount this problem, the construction of heterojunction structures for bismuth oxyhalides with other semiconductor were performed, which could further facilitate the charge separation through interfacial transporting, and sometimes strengthen the visible light harvesting of the materials [33–35]. For example, Zheng et al. prepared  $\text{WO}_3/\text{Bi}_{12}\text{O}_{17}\text{Cl}_2$  hybrids by a facile hydrothermal method, which exhibited enhanced photocatalytic performances for Rhodamine B (RhB) degradation under visible light [36]. Huang and co-workers fabricated  $\text{Bi}_4\text{O}_5\text{I}_2/\text{Bi}_5\text{O}_7\text{I}$  phase-junction photocatalyst by a calcination method, which possessed promoted performances for tetracycline hydrochloride, bisphenol A, and RhB degradations [37]. Bai et al. reported the synthesis of  $\text{g-C}_3\text{N}_4/\text{Bi}_4\text{O}_5\text{I}_2$  heterojunction with enhanced photocatalytic reduction activity

for  $\text{CO}_2$  conversion [38]. Obviously, the construction of heterostructures for photocatalysts exhibited great promise in promoting the charge carrier separation, as well as the photocatalytic performances.

Inspired by these works, we report the fabrication of composition-tunable 3D hierarchical bismuth oxyiodides via a facile ionic liquid-assisted precipitation method at room temperature. Prepared by a non-calcined method, the larger surface areas as well as the 3D hierarchical structures would be beneficial for the adsorption of pollutants. The phase components in the hybrids have been elaborately adjusted. To clarify the relationship of phase components and photocatalytic performances, the degradation of *o*-phenylphenol (OPP) over different samples have been systematically tested under visible light illumination. Lastly, the possible photocatalytic mechanism was proposed based on the semiconductor energy band theory and photoelectrochemical property test results.

## 2. Experimental section

### 2.1. Synthesis of photocatalysts

In this work, two groups of bismuth oxyiodides photocatalysts (G1:  $\text{BiOI}/\text{Bi}_4\text{O}_5\text{I}_2$ , and G2:  $\text{Bi}_4\text{O}_5\text{I}_2/\text{Bi}_5\text{O}_7\text{I}$ ) were fabricated using a facile ionic liquid-assisted precipitation method at room temperature. The schematic illustration for the synthesis of  $\text{BiOI}/\text{Bi}_4\text{O}_5\text{I}_2$  and  $\text{Bi}_4\text{O}_5\text{I}_2/\text{Bi}_5\text{O}_7\text{I}$  hybrids was displayed in Fig. 1. Typically, 1 mmol  $\text{Bi}(\text{NO}_3)_3 \cdot 5\text{H}_2\text{O}$  (0.485 g) was firstly dissolved into a solution containing 9 mL distilled water and 1 mL acetic acid under continuous magnetic stirring to form solution A. Meanwhile, 1 mmol of ionic liquid  $[\text{Bmim}]I$  and certain amount of sodium hydroxide (NaOH) were dissolved into 10 mL of absolute ethanol to form solution B. And then, the solution B was added dropwise into solution A under vigorous stirring. After 1 h of continuous stirring, the precipitates were collected, washed five times with distilled water, and then dried at 80 °C overnight. By changing the amounts of NaOH added,  $\text{BiOI}/\text{Bi}_4\text{O}_5\text{I}_2$  and  $\text{Bi}_4\text{O}_5\text{I}_2/\text{Bi}_5\text{O}_7\text{I}$  hybrid photocatalysts with different contents were fabricated. The samples obtained by adding NaOH of 0, 0.050, 0.075, 0.100, 0.125, 0.150, 0.200, 0.250, 0.275, 0.300, 0.325, and 0.35 g have been labeled as S1, S2, S3, S4, S5, S6, S7, S8, S9, S10, S11, and S12, respectively. Pristine  $\text{BiOI}$ ,  $\text{Bi}_4\text{O}_5\text{I}_2$ , and  $\text{Bi}_5\text{O}_7\text{I}$  were also prepared with the same method and used as references.

### 2.2. Characterization of photocatalysts

The X-ray diffraction (XRD) patterns of the products were recorded on a D8 Advance X-ray diffractometer employing Ni-filtered  $\text{Cu K}\alpha$  radiation. The chemical states of the obtained bismuth oxyiodide hybrids were investigated by X-ray photoelectron spectroscopy (XPS)

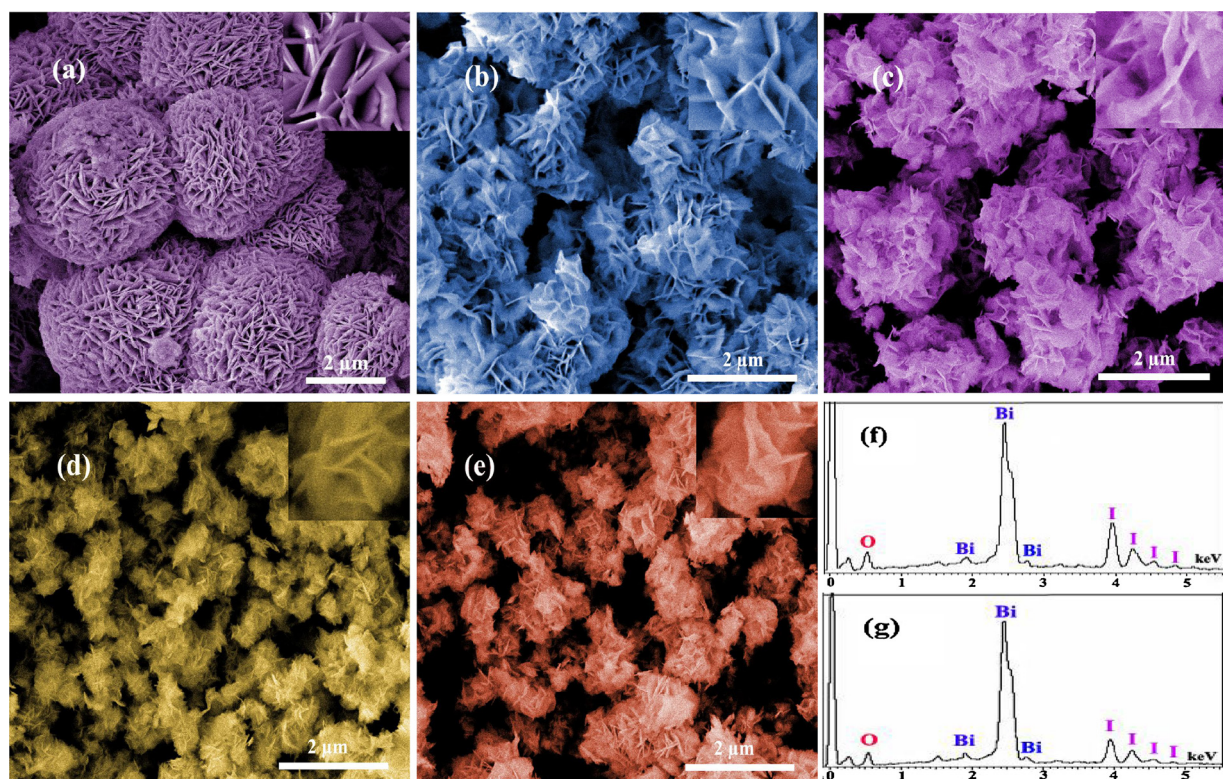


Fig. 3. SEM images of BiOI (a), S5 hybrid (b), Bi<sub>4</sub>O<sub>5</sub>I<sub>2</sub> (c), S9 hybrid (d), and Bi<sub>5</sub>O<sub>7</sub>I (e) with corresponding SEM-EDS spectrum of Bi<sub>4</sub>O<sub>5</sub>I<sub>2</sub> (f) and Bi<sub>5</sub>O<sub>7</sub>I (g).

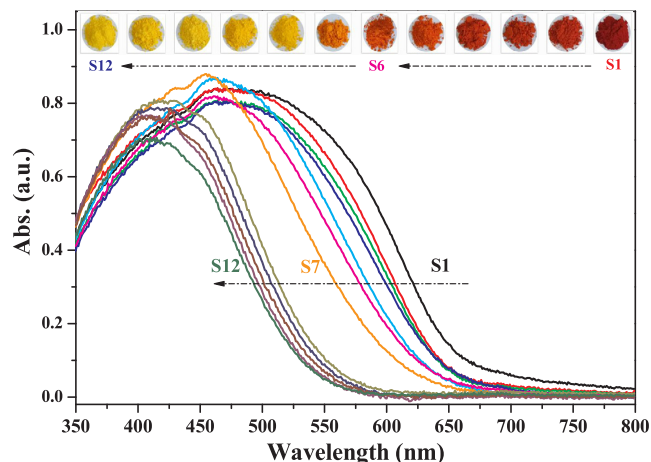


Fig. 4. DRS absorption spectra of two groups of bismuth oxyiodide hybrids.

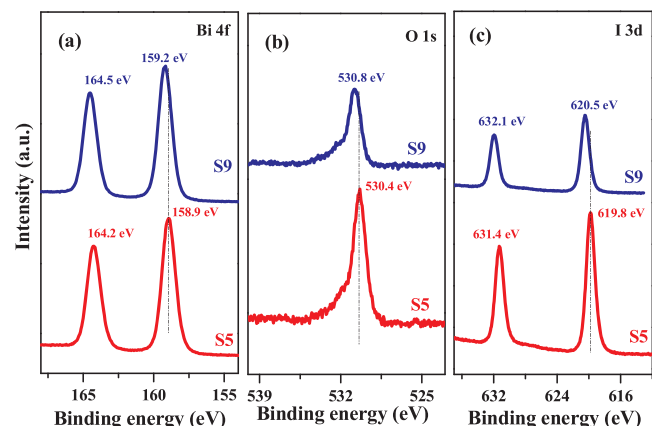


Fig. 5. High-resolution XPS spectra of Bi4f (a), O1s (b), I3d (c), and the survey spectrum (d) for S5 and S9 hybrids.

using an ESCALAB 250 apparatus (Thermo Fisher Scientific). The morphology was surveyed by a scanning electron microscope (FEI, NanoSEM 230). UV-vis diffuse reflectance spectra (DRS) were recorded using a UV-vis spectrophotometer (Cary 500, Varian, and USA). The total organic carbon (TOC) was measured with an Elementar-liqui TOC analyzer. The photocurrent and the electrochemical impedance spectroscopy (EIS) of the products were measured using an electrochemical station (Chenhua Instruments, CHI660D). The reactive species were detected by a Bruker model A300 spectrometer (Bruker Instruments, Inc.) with a 500 W Xe-arc lamp equipped with two cut-off filters ( $420 \text{ nm} < \lambda < 800 \text{ nm}$ ) as visible light source. Photoluminescence (PL) spectra were recorded on a Horiba Scientific FluoroMax-4 spectrophotofluorometer.

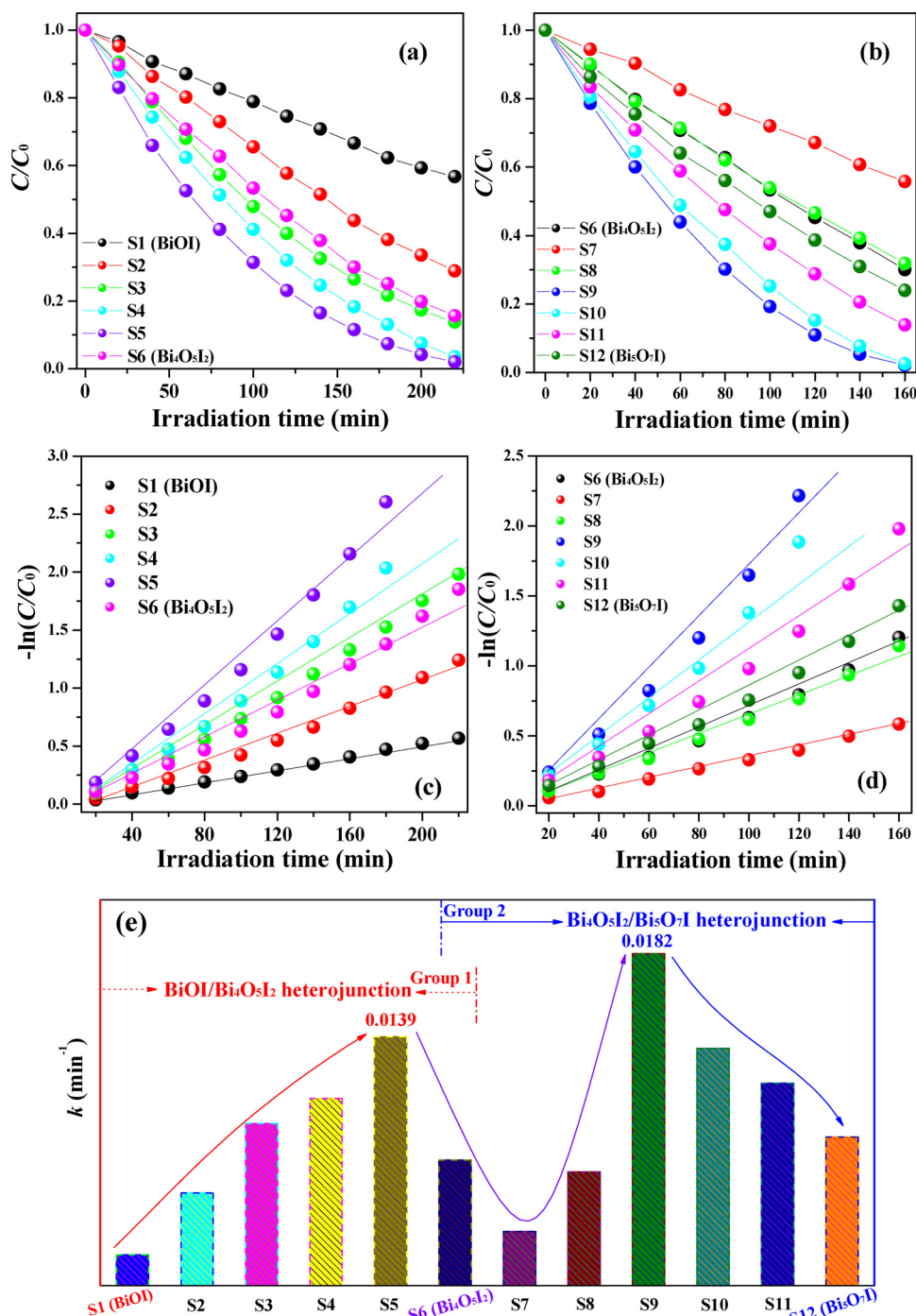


Fig. 6. The normalized concentration changes of OPP ( $30 \text{ mg L}^{-1}$ ) under visible light over G1 of BiOI/Bi<sub>4</sub>O<sub>5</sub>I<sub>2</sub> (a) and G2 of Bi<sub>4</sub>O<sub>5</sub>I<sub>2</sub>/Bi<sub>5</sub>O<sub>7</sub>I (b) hybrids; Kinetic fit curves for OPP degradation over G1 (c) and G2 (d) catalysts; The corresponding degradation rate constants over different samples (e).

### 2.3. Photocatalytic decomposition

The photocatalytic performances of the bismuth oxyiodides heterojunction photocatalysts were evaluated by decomposing OPP and 4-*tert*-butylphenol (PTBP) under visible light. A 500 W halogen lamp (Philips Electronics) combined with two cut-off filters has been used as the light source ( $420 \text{ nm} < \lambda < 800 \text{ nm}$ ). In a typical reaction, 40 mg of catalyst powders was dispersed into 80 mL of the contaminant solution. Before light irradiating, the suspension was firstly stirred for 60 min in dark to ensure the establishment of adsorption-desorption equilibrium. Then, the contaminant solution containing photocatalyst was irradiated by visible light. During this period, approximately

2.0 mL of the reaction solution was extracted at specified time and centrifuged to remove the catalyst powders. The residual pollutant concentration was measured by a UV-vis spectroscopy (PerkinElmer lambda 35, USA).

## 3. Results and discussion

### 3.1. Structural and morphology characterizations

Fig. 2 displays the XRD patterns of the obtained pristine BiOI, Bi<sub>4</sub>O<sub>5</sub>I<sub>2</sub>, Bi<sub>5</sub>O<sub>7</sub>I, and their hybrids with different contents. As we can see, the diffraction peaks of pristine BiOI prepared match well with

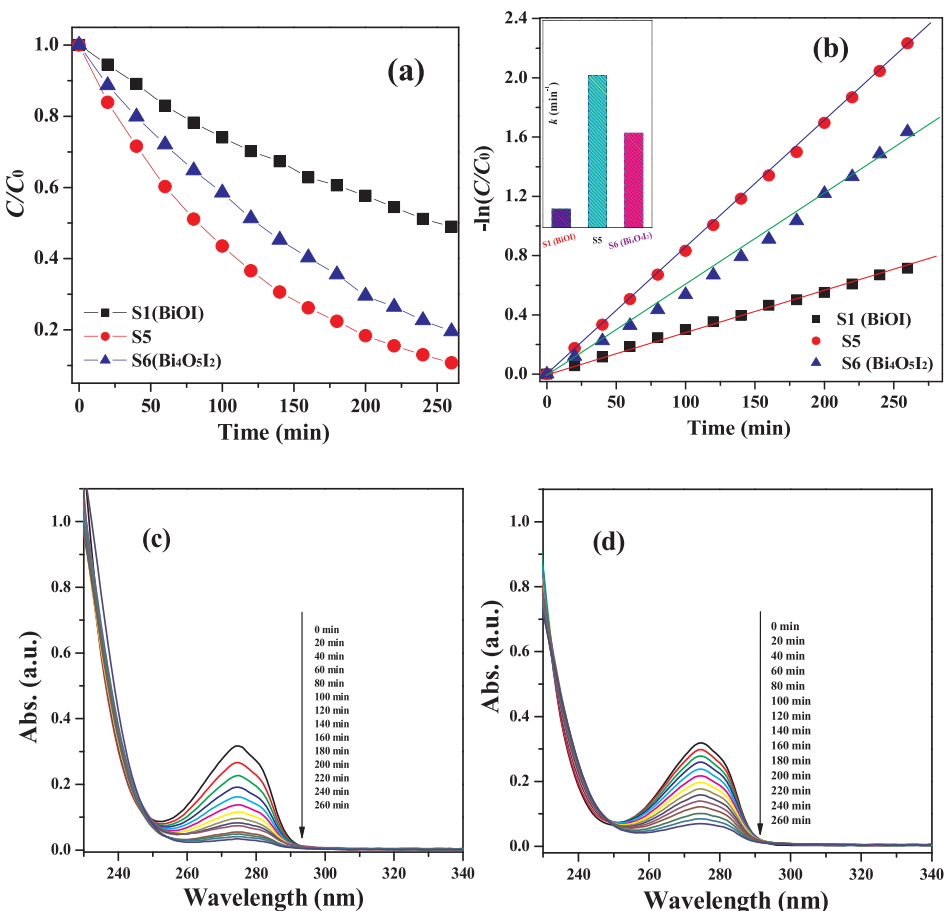


**Fig. 7.** The photocatalytic degradation curves of PTBP ( $30 \text{ mg L}^{-1}$ ) over BiOI, Bi<sub>4</sub>O<sub>5</sub>I<sub>2</sub>, and S5 hybrid (a); Kinetic fit curves for PTBP degradation over BiOI, Bi<sub>4</sub>O<sub>5</sub>I<sub>2</sub>, and S5 hybrid (b); UV-vis spectral changes of PTBP in the presence of S5 (c) and S9 hybrid (d) as a function of irradiation time.

tetragonal phase of BiOI (JCPDS card no. 10-0445) [39]. However, when small amount of NaOH was introduced during the fabrication procedure, BiOI/Bi<sub>4</sub>O<sub>5</sub>I<sub>2</sub> hybrids would be obtained. It was observed that the diffraction peak located at  $28.3^\circ$  was gradually widened along with the increase of NaOH amounts. When  $0.150 \text{ g}$  of NaOH was added, all the diffraction peaks of the product were well-indexed to pure phase of Bi<sub>4</sub>O<sub>5</sub>I<sub>2</sub> according to previous reports [40]. Interestingly, when a bit more of NaOH was further introduced, the product would partially exhibit phase transition from Bi<sub>4</sub>O<sub>5</sub>I<sub>2</sub> into Bi<sub>5</sub>O<sub>7</sub>I [41]. And thus, through elaborately governing the amounts of NaOH added, two series of composition-tunable 3D hierarchical bismuth oxyiodides hybrids have been fabricated using present method.

The morphology and microscopic structures of the bismuth oxyiodides were investigated by using SEM. Fig. 3a depicts the SEM image of pristine BiOI. As it shows, the obtained BiOI mainly exhibits microsphere-like morphology with diameters of  $2\text{--}5 \mu\text{m}$ . And the flower-like microspheres were composed of countless plates. Fig. 3b depicts the SEM image for BiOI/Bi<sub>4</sub>O<sub>5</sub>I<sub>2</sub> hybrids (typical S5 hybrid). Obviously, S5 hybrid did not possess sphere-like morphology as that for pristine BiOI. The obtained nanoplates were assembled together to form 3D hierarchical structures with relatively smaller sizes. As for the bare Bi<sub>4</sub>O<sub>5</sub>I<sub>2</sub> (S6 sample), it also exhibited hierarchical structures assembled by numerous of plates (Fig. 3c). For the Bi<sub>4</sub>O<sub>5</sub>I<sub>2</sub>/Bi<sub>5</sub>O<sub>7</sub>I hybrids, the SEM image of the typical S9 hybrid was shown in Fig. 3d. As we can see, numerous of plates were self-assembled to form flower-like spheres with diameters of  $20\text{--}500 \text{ nm}$ . The SEM image of S12 (Bi<sub>5</sub>O<sub>7</sub>I) shown in Fig. 3e shows that lots of plates were accumulated severely to form hierarchical structures. The corresponding EDS spectrum of S6 (Bi<sub>4</sub>O<sub>5</sub>I<sub>2</sub>, Fig. 3f) and S12 (Bi<sub>5</sub>O<sub>7</sub>I, Fig. 3g) shows that only signals for element Bi,

O, and I have been detected, indicating the high purity of the products. The analysis above proved that through elaborately governing the addition of NaOH, the compositions, morphologies, as well as the particle sizes of the products all had been tuned gradually.

### 3.2. DRS and XPS characterization

The optical property of photocatalyst could severely influence its photocatalytic activity, which was largely determined by the light absorption and utilization. So, the optical properties of the obtained samples (BiOI, Bi<sub>4</sub>O<sub>5</sub>I<sub>2</sub>, Bi<sub>5</sub>O<sub>7</sub>I, and their hybrids) were characterized using a UV-vis diffuse reflectance spectroscopy. As shown in Fig. 4, all of the samples have exhibited strong absorption abilities in the visible light region, but their absorption edges have been gradually tuned from  $660$  to  $550 \text{ nm}$ . A paragraph of the samples shown at the top of Fig. 4 displays the gradual color change from brick red to light yellow.

XPS was used to investigate the surface composition and electronic structure of the composites. Fig. 5a shows the high-resolution XPS spectra of Bi 4f for S5 and S9 hybrids, in which two peaks assigned to Bi4f<sub>7/2</sub> and Bi4f<sub>5/2</sub> have been observed. For S5 sample, the binding energy of Bi4f<sub>7/2</sub> and Bi4f<sub>5/2</sub> peak was about  $158.9$  and  $164.2 \text{ eV}$ , respectively. As for the S9 sample, the two Bi4f peaks were slightly shifted to higher binding energy for about  $0.3 \text{ eV}$ , indicating the different chemical environment of Bi<sup>3+</sup> in the two hybrid samples [42]. Meanwhile, the peak in the O1s spectra of S9 hybrid shown in Fig. 5b also showed a  $0.4 \text{ eV}$  shift to higher binding energy compared with that of S5 hybrid. As for the I3d spectra in Fig. 5c, the two peaks of I3d<sub>3/2</sub> and I3d<sub>5/2</sub> for S9 hybrid was centered at  $632.1 \text{ eV}$  and  $620.5 \text{ eV}$ , respectively. While the peaks for S5 hybrid was located at  $631.4 \text{ eV}$  and

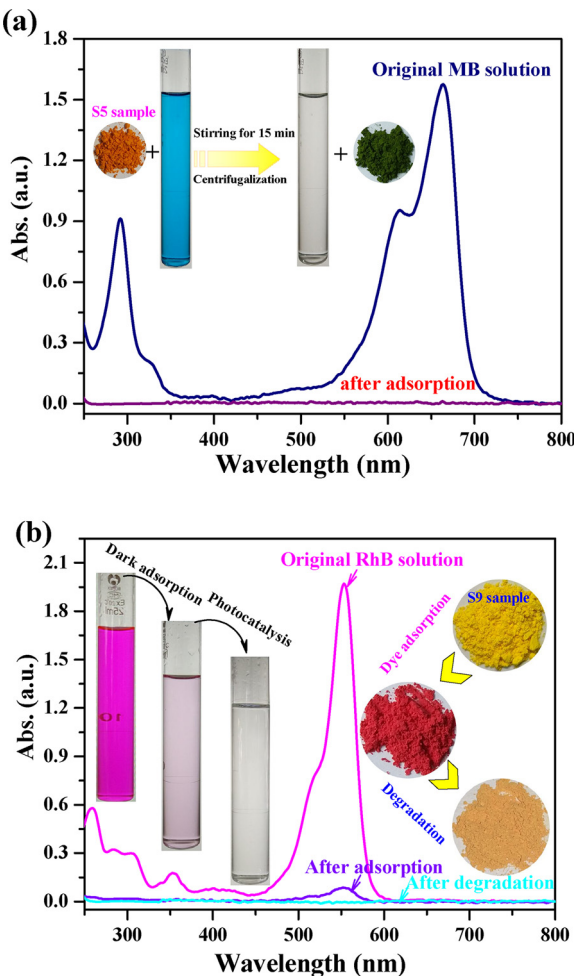


Fig. 8. The adsorption of MB (80 mL, 10 mg L<sup>-1</sup>) over S5 hybrid (40 mg) in dark (a); the adsorption of RhB (80 mL, 2 × 10<sup>-5</sup> M) over S9 hybrid (40 mg) in dark and the photocatalytic degradation of RhB over S9 hybrid under visible light (b).

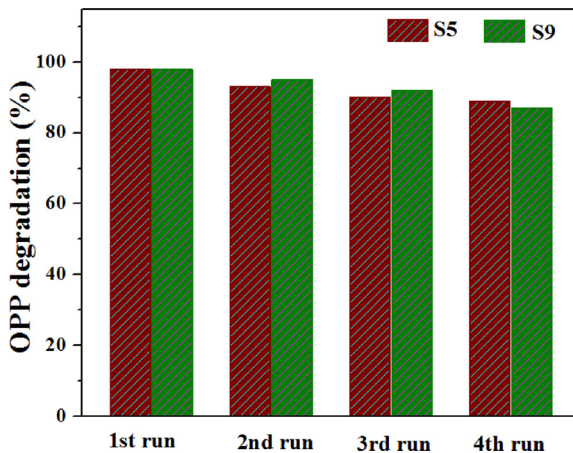


Fig. 9. (a) Recycling runs of the photocatalytic degradation of OPP over S5 and S9 hybrid photocatalyst under visible light irradiation.

619.8 eV with lower binding energy. Fig. 5d displays the XPS survey spectra for S5 and S9 hybrids. As it shows, only signals attributed to element Bi, O, and I were observed, indicating the high purity of the obtained samples.

### 3.3. Photocatalytic performances and adsorption of dyes

The photocatalytic activities of BiOI/Bi<sub>4</sub>O<sub>5</sub>I<sub>2</sub> and Bi<sub>4</sub>O<sub>5</sub>I<sub>2</sub>/Bi<sub>5</sub>O<sub>7</sub>I hybrids were mainly evaluated by the decomposition of OPP (30 mg L<sup>-1</sup>) under visible light illumination. In the degradation experiments, pristine BiOI, Bi<sub>4</sub>O<sub>5</sub>I<sub>2</sub>, and Bi<sub>5</sub>O<sub>7</sub>I also have been used as references. Firstly, the degradations of OPP over BiOI/Bi<sub>4</sub>O<sub>5</sub>I<sub>2</sub> hybrids have been investigated, and the OPP removal ratios after 220 min of reaction were shown in Fig. 6a. As we can see, the activity of bare BiOI (S1) was very poor, and the degradation ratio of OPP was only about 43%. On the contrary, all of the BiOI/Bi<sub>4</sub>O<sub>5</sub>I<sub>2</sub> hybrids have exhibited remarkably enhanced activities compared with pristine BiOI. It was also found that the content of BiOI to Bi<sub>4</sub>O<sub>5</sub>I<sub>2</sub> has great influence on the photocatalytic performances. The activity of the samples was gradually enhanced in the order of S1(BiOI) < S2 < S6(Bi<sub>4</sub>O<sub>5</sub>I<sub>2</sub>) < S3 < S4 < S5. That is to say, for the G1 BiOI/Bi<sub>4</sub>O<sub>5</sub>I<sub>2</sub> hybrids, the S5 sample possessed the optimal activity, and the degradation ratio of OPP was nearly up to 98% after reaction, which was also higher than that for pristine Bi<sub>4</sub>O<sub>5</sub>I<sub>2</sub> (84%) under identical conditions. In addition, the Bi<sub>4</sub>O<sub>5</sub>I<sub>2</sub>/Bi<sub>5</sub>O<sub>7</sub>I hybrids in G2 all exhibited stronger photocatalytic performance compared with that of BiOI/Bi<sub>4</sub>O<sub>5</sub>I<sub>2</sub> hybrids in G1. As we can see in Fig. 6b, the photocatalytic degradation of OPP became more efficient over Bi<sub>4</sub>O<sub>5</sub>I<sub>2</sub>/Bi<sub>5</sub>O<sub>7</sub>I hybrids, and the complete removal of OPP has been accomplished within 160 min of reaction. Similarly, the contents of Bi<sub>4</sub>O<sub>5</sub>I<sub>2</sub>/Bi<sub>5</sub>O<sub>7</sub>I could greatly influence the photocatalytic activity of the hybrids. And the activity of the samples was in the order of S7 < S8 < S6(Bi<sub>4</sub>O<sub>5</sub>I<sub>2</sub>) < S12(Bi<sub>5</sub>O<sub>7</sub>I) < S11 < S10 < S9. So, the S9 hybrid has exhibited the best activity toward OPP degradation. The kinetic behaviors for OPP decomposition over BiOI/Bi<sub>4</sub>O<sub>5</sub>I<sub>2</sub> and Bi<sub>4</sub>O<sub>5</sub>I<sub>2</sub>/Bi<sub>5</sub>O<sub>7</sub>I hybrids also have been investigated. As shown in Fig. 6c and d, the photocatalytic degradation processes of OPP over different samples all fitted well with the first-order reaction dynamic model [43]:

$$-\ln(C/C_0) = kt$$

In this equation,  $C_0$  is the OPP concentration after adsorption/desorption equilibrium establishment, while  $C$  and  $k$  stand for the temporal concentration of OPP at reaction time  $t$  and the degradation rate constant. Fig. 6e shows the calculated degradation rate constants for OPP degradations over different samples. For BiOI/Bi<sub>4</sub>O<sub>5</sub>I<sub>2</sub> hybrids in G1, the S5 sample exhibited the highest degradation rate constant of 0.0139 min<sup>-1</sup>, which was nearly about 5.3 times higher than that of pristine BiOI. For Bi<sub>4</sub>O<sub>5</sub>I<sub>2</sub>/Bi<sub>5</sub>O<sub>7</sub>I hybrids in G2, the highest degradation rate constant was observed over S9 hybrid, which was about 2.4 times higher than that of pristine Bi<sub>4</sub>O<sub>5</sub>I<sub>2</sub>. Furthermore, the mineralization of OPP over different samples was measured to understand their oxidation efficiencies. As shown in Fig. S1, the TOC removal ratios over different samples were various after the photocatalytic degradation under visible light irradiation. Apparently, for the first group, the maximum TOC removal was approximately 68% for the S5 hybrid after 220 min irradiation, while the S9 hybrid in the second group possessed the highest TOC removal ratio of 64% after 160 min of reaction. That is to say, during the photocatalytic degradation process, OPP molecules could be mineralized over bismuth oxyiodide heterojunction photocatalysts under visible light illumination.

PTBP, another kind of phenolic compounds, was also used to investigate the photocatalytic activities of the hybrids. Fig. 7a shows the PTBP (30 mg L<sup>-1</sup>) degradation over S5 hybrid using pristine BiOI and Bi<sub>4</sub>O<sub>5</sub>I<sub>2</sub> as references. Obviously, the photocatalytic decomposition of PTBP over S5 was much more efficient. After 260 min of reaction, the removal ratio over S5 was about 90%, while that over bare BiOI and Bi<sub>4</sub>O<sub>5</sub>I<sub>2</sub> was only about 51% and 80%, respectively. Fig. 7b shows that the degradation of PTBP also followed the first-order reaction dynamic model, and the degradation rate constant for S5 sample was about 3.0 and 1.4 times higher than that of bare BiOI and Bi<sub>4</sub>O<sub>5</sub>I<sub>2</sub>, respectively.

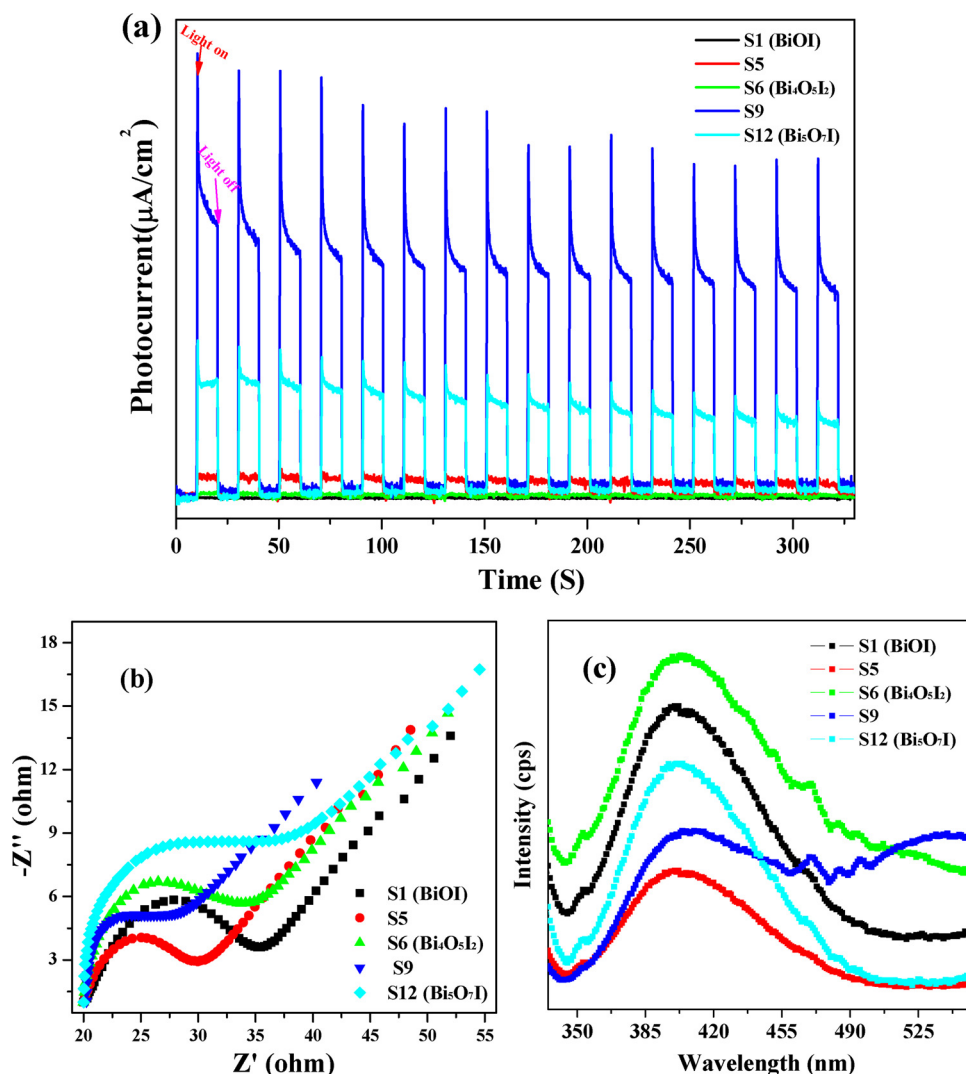


Fig. 10. Photocurrent responses (a), EIS plots (b), and PL emission (c) of  $\text{BiOI}$ ,  $\text{Bi}_4\text{O}_5\text{I}_2$ ,  $\text{Bi}_5\text{O}_7\text{I}$ , S5 and S9 samples.

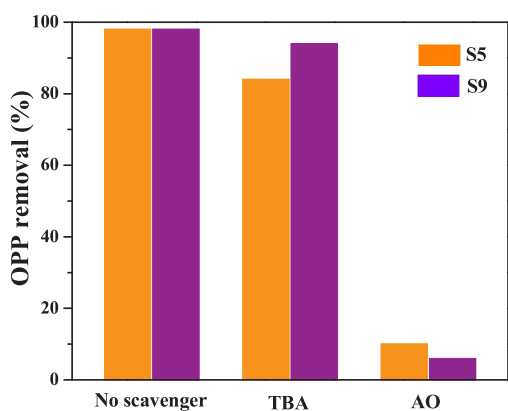


Fig. 11. Effects of various trapping agents on the photocatalytic degradation of OPP over S5 and S9 samples.

Fig. 7c depicts the temporal spectral changes of PTBP mediated by S5 hybrid. The main absorption peak located at 283 nm was belonged to PTBP. During the whole degradation process, the peak intensity was gradually decreased with degradation time. In addition, a similar situation also has been observed for the photocatalytic decomposition of PTBP over S9 hybrid (see Fig. 7d). All these degradation results show that  $\text{BiOI}/\text{Bi}_4\text{O}_5\text{I}_2$  and  $\text{Bi}_4\text{O}_5\text{I}_2/\text{Bi}_5\text{O}_7\text{I}$  hybrid photocatalysts could treat

phenolic compounds in water very efficiently under visible light.

Besides phenolic compounds, two kinds of dyes, such as RhB and methylene blue (MB), also have been used to evaluate the adsorption capability as well as the photocatalytic activity of S5 and S9 samples. Fig. 8a shows the adsorption of MB solution (80 mL, 10 mg  $\text{L}^{-1}$ ) over S5 hybrid (40 mg). As we can see, the absorption peaks of MB were nearly completely disappeared only after 15 min of stirring in dark, indicating the strong adsorptive ability of S5 hybrid toward MB molecules due to its 3D hierarchical architectures. The decolorization of MB solution also could be proved by the photograph inset in Fig. 8a. Accordingly, the color of S5 powders was changed into atrovirens from brick red, revealing the large adsorption quantity of MB molecules on its surfaces. In addition, the adsorptive ability of S9 hybrid toward RhB solution ( $2 \times 10^{-5}$  M) also has been evaluated. As shown in Fig. 8b, the S9 hybrid exhibited strong adsorptive ability toward RhB molecules in water. After 15 min of stirring in dark, the red color of RhB solution became very light. The adsorption ratio of RhB was calculated to be 96%. The residual 4% of RhB in the solution could be decomposed by S9 hybrid within 20 min of illumination by visible light. The photograph inset in Fig. 8b also displays the color changing of S9 sample. After adsorption of RhB molecules, the color of S9 hybrid changed to deepred from yellow, which was finally changed to light-aurantiacus after 20 min of light illumination, indicating the complete removal of RhB by photocatalytic degradation. For comparison, the adsorption properties of different catalysts towards the colorless OPP also have

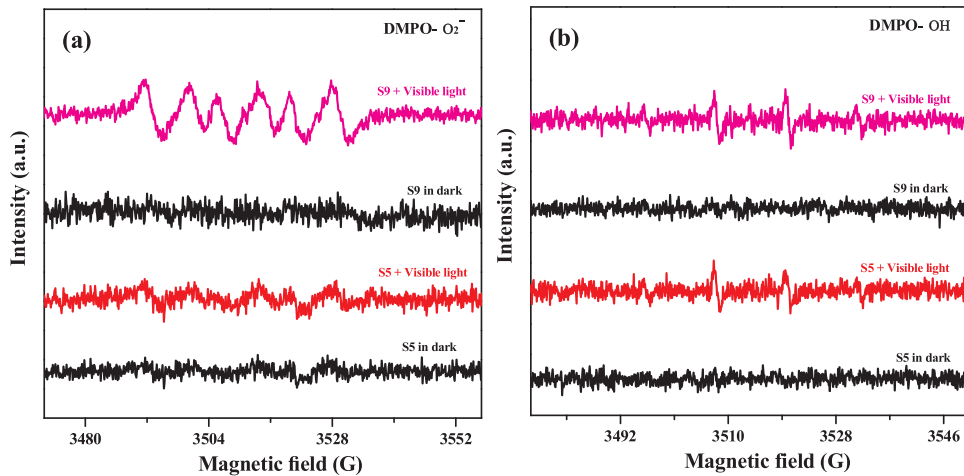


Fig. 12. ESR signals of the DMPO-trapped  $\cdot\text{O}_2^-$  (a) and DMPO-trapped  $\cdot\text{OH}$  (b) in the S5 and S9 hybrid system.

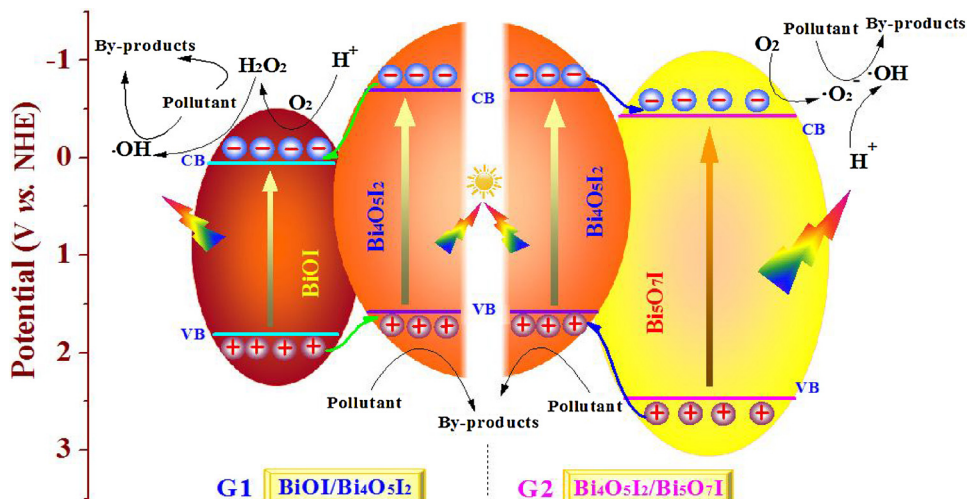


Fig. 13. The proposed photocatalytic degradation mechanisms over G1 of  $\text{BiOI}/\text{Bi}_4\text{O}_5\text{I}_2$  and G2 of  $\text{Bi}_4\text{O}_5\text{I}_2/\text{Bi}_5\text{O}_7\text{I}$  hybrids under visible light illumination.

been investigated. As shown in Fig. S3, the absorption ratios of OPP over different samples varied from 9% to 14%. So, the absorption of colorless organic pollutants over bismuth oxyiodide heterojunction was greatly weaker than that of dyes.

The activity durability of S5 and S9 hybrids were evaluated by recycling the used catalyst. As shown in Fig. 9, only low activity loss was observed during the degradation process of OPP over S5 and S9 after four cycles. And thus, the  $\text{BiOI}/\text{Bi}_4\text{O}_5\text{I}_2$  and  $\text{Bi}_4\text{O}_5\text{I}_2/\text{Bi}_5\text{O}_7\text{I}$  hybrids not only possessed efficient photocatalytic activity, but also maintained good photo-stability under visible light. Additionally, the XRD patterns of the fresh and used samples (hybrid S5 and S9) were obtained to study the chemical stability of the products. As shown in Fig. S2, the XRD patterns of the fresh and used samples were nearly the same, indicating that the crystal phase of hybrid S5 and S9 were stable under reaction conditions.

#### 3.4. Degradation mechanism

For hybrid photocatalysts, the interfacial charge separation together with the materials' energy band potentials determined the kinds and amounts of active species generated in the system, which would severely affect the degradation rates of contaminants. Hence, the charge separation efficiency over  $\text{BiOI}/\text{Bi}_4\text{O}_5\text{I}_2$  and  $\text{Bi}_4\text{O}_5\text{I}_2/\text{Bi}_5\text{O}_7\text{I}$  hybrids was firstly investigated by photocurrent, electrochemical impedance spectroscopy, and photoluminescence. Fig. 10a depicts the photocurrent-

time responses with light on/off cycles over different samples. Obviously, the S5 hybrid in G1 shows a higher current intensity compared to individual  $\text{BiOI}$  and  $\text{Bi}_4\text{O}_5\text{I}_2$ , while the S9 hybrid displays the highest current intensity in G2. As stronger photocurrent intensity predicates higher separation efficiency of electron/hole pairs [44], the charge separation efficiency over S5 and S9 hybrids should be severely promoted compared to single-phase  $\text{BiOI}$ ,  $\text{Bi}_4\text{O}_5\text{I}_2$ , and  $\text{Bi}_5\text{O}_7\text{I}$ . These results were also in good agreement with the enhanced photocatalytic activities for OPP degradation. Fig. 10b depicts the EIS Nyquist plots recorded over different samples. As the smaller arc radius of the plot indicates the lower interface layer resistance [45], the charge separation and transfer over S5 hybrid in G1 would be promoted compared with bare  $\text{BiOI}$  and  $\text{Bi}_4\text{O}_5\text{I}_2$ , while the S9 hybrid in G2 also possessed accelerated charge transport and promoted separation efficiency. The PL emission spectra in Fig. 10c reveal the charge separation efficiency over various products more intuitively. It shows that the PL emission intensity for S5 hybrid was lower than that of bare  $\text{BiOI}$  and  $\text{Bi}_4\text{O}_5\text{I}_2$  in G1, while that for S9 sample was the lowest compared with pristine  $\text{Bi}_4\text{O}_5\text{I}_2$  and  $\text{Bi}_5\text{O}_7\text{I}$  in G2. That is to say, the recombination of charge carriers have been greatly depressed over S5 and S9 hybrids because of the interfacial charge transfer in the hybrids. All these results disclosed that the enhanced charge separation result in the activity enhancement of the bismuth iodides hybrids.

Secondly, the active species generated in the photocatalytic process also played an important role in determining the degradation rates of

contaminants. Therefore, trapping experiments were performed to investigate the influences of different radical scavengers on the OPP degradations under visible light. As shown in Fig. 11, when *Tert*-butanol (TBA) was used to capture  $\cdot\text{OH}$  [46], the degradation rate of OPP over S5 and S9 samples only exhibited slight decrease. However, when ammonium oxalate (AO) was introduced as hole scavenger [47], the degradation rates have been severely inhibited, indicating that the pollutants were mainly decomposed by holes that generated in the system. In addition, ESR technique was also performed to investigate the generation of  $\cdot\text{O}_2^-$  and  $\cdot\text{OH}$  radicals in the system using 5,5-dimethyl-1-pyrroline N-oxide (DMPO) as a radical trapping reagents [48,49]. Fig. 12 displays the ESR spectra of S5 and S9 hybrids. As we can see in Fig. 12a, no ESR signals of  $\cdot\text{O}_2^-$  have been observed when the system containing S5 or S9 sample was in dark. However, when the system was irradiated by visible light, six characteristic peaks of DMPO- $\cdot\text{O}_2^-$  could be obviously observed for S9 sample, while the signals for S5 hybrid was relatively weaker. The strong signal intensity indicated that large amounts of  $\cdot\text{O}_2^-$  radicals were generated under visible light. Fig. 12b displays the ESR signals of  $\cdot\text{OH}$  in an aqueous dispersion containing S5 or S9 sample. Similarly, no ESR signals were observed without light illumination. While irradiated by visible light, weak signals for DMPO- $\cdot\text{OH}$  species could be observed for the system containing S5 or S9 sample, revealing that only a small amount of  $\cdot\text{OH}$  radicals were produced in the photocatalytic system. These results were also well coincided with the results of the trapping experiments. All the experiment results discussed above might prove that holes and  $\cdot\text{O}_2^-$  radicals were the major reactive species that responsible for the degradation of pollutants.

Based on the energy band theory and trapping experiment results, the possible photocatalytic degradation mechanisms for the BiOI/Bi<sub>4</sub>O<sub>5</sub>I<sub>2</sub> and Bi<sub>4</sub>O<sub>5</sub>I<sub>2</sub>/Bi<sub>5</sub>O<sub>7</sub>I hybrids were proposed (Fig. 13). Previous literature reported that the band energy levels of BiOI, Bi<sub>4</sub>O<sub>5</sub>I<sub>2</sub>, and Bi<sub>5</sub>O<sub>7</sub>I are as follows [37]: BiOI ( $E_{\text{CB}} = 0.07$  eV,  $E_{\text{VB}} = 1.82$  eV), Bi<sub>4</sub>O<sub>5</sub>I<sub>2</sub> ( $E_{\text{CB}} = -0.68$  eV,  $E_{\text{VB}} = 1.61$  eV), and Bi<sub>5</sub>O<sub>7</sub>I ( $E_{\text{CB}} = -0.47$  eV,  $E_{\text{VB}} = 2.45$  eV). For BiOI/Bi<sub>4</sub>O<sub>5</sub>I<sub>2</sub> hybrids in G1, both BiOI ( $E_g = 1.75$  eV) and Bi<sub>4</sub>O<sub>5</sub>I<sub>2</sub> ( $E_g = 2.29$  eV) could be excited by visible light, resulting in the generation of holes in their VB as well as electrons in their CB. Because the CB potential of Bi<sub>4</sub>O<sub>5</sub>I<sub>2</sub> was more negative than that of BiOI, the electrons stored in the CB of Bi<sub>4</sub>O<sub>5</sub>I<sub>2</sub> would transfer into the CB of BiOI through the interfacial heterojunction. Subsequently, the holes stored in the VB of BiOI would transfer into the CB of Bi<sub>4</sub>O<sub>5</sub>I<sub>2</sub> that with a relatively higher band potential. Because the CB position of BiOI is more positive than  $\text{O}_2^-/\cdot\text{O}_2^-$  ( $-0.33$  V vs. NHE) [50], the electrons stored there were not able to react with  $\text{O}_2$  to produce  $\cdot\text{O}_2^-$ . Alternatively, the electrons would react with  $\text{H}^+$  and dissolved  $\text{O}_2$  to produce  $\text{H}_2\text{O}_2$ , which would further react to produce  $\cdot\text{OH}$ . Additionally, the holes stored in the VB of Bi<sub>4</sub>O<sub>5</sub>I<sub>2</sub> were not able to oxidize  $\text{OH}^-$  to produce  $\cdot\text{OH}$  because its  $E_{\text{VB}}$  was too negative compared with  $\cdot\text{OH}/\text{OH}^-$  ( $+2.27$  V vs. NHE) [51]. And then, the holes could oxidize surface-absorbed organic pollutants directly. As for the Bi<sub>4</sub>O<sub>5</sub>I<sub>2</sub>/Bi<sub>5</sub>O<sub>7</sub>I hybrids in G2, a similar degradation mechanism was proposed except that the  $E_{\text{CB}}$  of Bi<sub>5</sub>O<sub>7</sub>I was more negative than that for  $\text{O}_2^-/\cdot\text{O}_2^-$  ( $-0.33$  V). And thus, the electrons that transferred from Bi<sub>4</sub>O<sub>5</sub>I<sub>2</sub> into the CB of Bi<sub>5</sub>O<sub>7</sub>I would react with  $\text{O}_2$  to produce  $\cdot\text{O}_2^-$ . This result was also well coincided with the ESR characterization results. The photo-generated  $\cdot\text{O}_2^-$  and holes stored in the VB of Bi<sub>4</sub>O<sub>5</sub>I<sub>2</sub> both could oxidize organic pollutants directly, resulting in the efficient removal of contaminants from water.

#### 4. Conclusions

In summary, two groups of bismuth oxyiodides hybrids were successfully fabricated using a facile ionic liquid-assisted precipitation method. Through elaborately adjusting the component of the hybrids, their optical properties as well as photocatalytic performances have been gradually tuned. In the photocatalytic degradation of OPP under

visible light, the S5 and S9 hybrids exhibited remarkably promoted performances. The enhanced activity of these hybrid materials should be attributed to their promoted charge separation efficiency as well as their suitable band positions. The trapping experiments and ESR measurements confirmed the generation of  $\cdot\text{OH}$ ,  $\cdot\text{O}_2^-$ , and holes, which were responsible for the degradation of phenolic pollutants in water.

#### Acknowledgment

This work was financially supported by the Shandong Provincial Natural Science Foundation, China (No. ZR2016BQ12, ZR2014BL017), NSFC (No. 21505051 and 21175057), the Science Foundation for Post Doctorate Research from the University of Jinan (XBH1708), Project funded by China Postdoctoral Science Foundation (No. 2017M612172), and the Open Project Program of the State Key Laboratory of Photocatalysis on Energy and Environment (Grant No. SKLPEE-KF201709).

#### Appendix A. Supplementary data

Supplementary material related to this article can be found, in the online version, at doi:<https://doi.org/10.1016/j.apcatb.2018.04.010>.

#### References

- X. Qu, M. Tian, B.Q. Liao, A.C. Chen, Enhanced electrochemical treatment of phenolic pollutants by an effective adsorption and release process, *Electrochim. Acta* 55 (2010) 5367–5374.
- X. Zhu, S. Shi, J. Wei, F. Lv, H. Zhao, J. Kong, Q. He, J. Ni, Electrochemical oxidation characteristics of p-substituted phenols using a boron-doped diamond electrode, *Environ. Sci. Technol.* 41 (2007) 6541–6546.
- H. Zhang, L.X. Zhao, F.L. Geng, L.H. Guo, B. Wan, Y. Yang, Carbon dots decorated graphitic carbon nitride as an efficient metal-free photocatalyst for phenol degradation, *Appl. Catal. B Environ.* 180 (2016) 656–662.
- S.G. Anju, S. Yesodharan, E.P. Yesodharan, Zinc oxide mediated sonophotocatalytic degradation of phenol in water, *Chem. Eng. J.* 189–190 (2012) 84–93.
- J.D. Xiao, Y.B. Xie, Q.Z. Han, H.B. Cao, Y.J. Wang, F. Nawaz, F. Duan, Superoxide radical-mediated photocatalytic oxidation of phenolic compounds over  $\text{Ag}^+/\text{TiO}_2$ : influence of electron donating and withdrawing substituents, *J. Hazard. Mater.* 304 (2016) 126–133.
- Y. Hou, X.Y. Li, Q.D. Zhao, X. Quan, G.H. Chen, Electrochemically assisted photocatalytic degradation of 4-chlorophenol by  $\text{ZnFe}_2\text{O}_4$ -modified  $\text{TiO}_2$  nanotube array electrode under visible light irradiation, *Environ. Sci. Technol.* 44 (2010) 5098–5103.
- Y. Hu, D.Z. Li, F.Q. Sun, Y.Q. Weng, S.Y. You, Y. Shao, Temperature-induced phase changes in bismuth oxides and efficient photodegradation of phenol and p-chlorophenol, *J. Hazard. Mater.* 301 (2016) 362–370.
- J.J. Jiang, H.T. Wang, X.D. Chen, S. Li, T.F. Xie, D.J. Wang, Y.H. Lin, Enhanced photocatalytic degradation of phenol and photogenerated charges transfer property over BiOI-loaded ZnO composites, *J. Colloid Interface Sci.* 494 (2017) 130–138.
- N. Calace, E. Nardi, B.M. Petronio, M. Pietroletti, Adsorption of phenols by palmill sludges, *Environ. Pollut.* 118 (2002) 315–319.
- A. Hirata, M. Noguchi, N. Takeuchi, S. Tsuneda, Kinetics of biological treatment of phenolic wastewater in three-phase fluidized bed containing biofilm and suspended sludge, *Water Sci. Technol.* 38 (1998) 205–212.
- Akshay Jain, Sundaramurthy Jayaraman, Gurdev Singh, M.P. Srinivasan, Single step peroxidase extraction and oxidation of highly concentrated ethanol and phenol aqueous solutions using supercritical carbon dioxide, *J. Supercrit. Fluids* 116 (2016) 209–214.
- R.S. Juang, W.C. Huang, Y.H. Hsu, Treatment of phenol in synthetic saline wastewater by solvent extraction and two-phase membrane biodegradation, *J. Hazard. Mater.* 164 (2009) 46–52.
- F. Akbal, Sorption of phenol and 4-chlorophenol onto pumice treated with cationic surfactant, *J. Environ. Manage.* 74 (2005) 239–244.
- K. Kuśmierkiewicz, The removal of chlorophenols from aqueous solutions using activated carbon adsorption integrated with  $\text{H}_2\text{O}_2$  oxidation, *React. Kinet. Mech. Catal.* 119 (2016) 19–34.
- T. Wang, H.P. Zhao, H. Wang, B.T. Liu, C.Q. Li, Research on degradation product and reaction kinetics of membrane electro-bioreactor (MEBR) with catalytic electrodes for high concentration phenol wastewater treatment, *Chemosphere* 155 (2016) 94–99.
- C.L. Yu, W.Q. Zhou, H. Liu, Y. Liu, D.D. Dionysiou, Design and fabrication of microsphere photocatalysts for environmental purification and energy conversion, *Chem. Eng. J.* 287 (2016) 117–129.
- S. Ivanova, A. Penkova, M.C. Hidalgo, J.A. Navío, F. Romero-Sarria, M.Á. Centeno, J.A. Odriozola, Synthesis and application of layered titanates in the photocatalytic degradation of phenol, *Appl. Catal. B Environ.* 163 (2015) 23–29.
- H. Yin, X.X. Dai, M.Q. Zhu, F.H. Li, X.H. Feng, F. Liu, Fe-doped cryptomelane

synthesized by refluxing at atmosphere: structure, properties and photocatalytic degradation of phenol, *J. Hazard. Mater.* 296 (2015) 221–229.

[19] J. Li, X.Y. Wu, W.F. Pan, G.K. Zhang, H. Chen, Vacancy-rich monolayer  $\text{BiO}_{2-x}$  as a highly efficient UV, visible, and near-infrared responsive photocatalyst, *Angew. Chem. Int. Ed.* 57 (2) (2018) 491–495.

[20] M.Q. Fang, H.M. Jia, W.W. He, Y. Lei, L.Z. Zhang, Z. Zheng, Construction of flexible photoelectrochemical solar cells based on ordered nanostructural  $\text{BiOI}/\text{Bi}_2\text{S}_3$  heterojunction films, *Phys. Chem. Chem. Phys.* 17 (2015) 13531–13538.

[21] X.A. Dong, W.D. Zhang, Y.J. Sun, J.Y. Li, W.L. Cen, Z.H. Cui, H.W. Huang, F. Dong, Visible-light-induced charge transfer pathway and photocatalysis mechanism on Bi semimetal@defective  $\text{BiOB}$  hierarchical microspheres, *J. Catal.* 357 (2018) 41–50.

[22] S. Zhao, Y.W. Zhang, Y.M. Zhou, C. Zhang, X.L. Sheng, J.S. Fang, M.Y. Zhang, Reactable polyelectrolyte-assisted synthesis of  $\text{BiOCl}$  with enhanced photocatalytic activity, *ACS Sustain. Chem. Eng.* 5 (2) (2017) 1416–1424.

[23] C. Zeng, Y.M. Hua, Y.X. Guo, T.R. Zhang, F. Dong, X. Du, Y.H. Zhang, H.W. Huang, Achieving tunable photocatalytic activity enhancement by elaborately engineering composition-adjustable polynary heterojunctions photocatalysts, *Appl. Catal. B Environ.* 194 (2016) 62–73.

[24] J.X. Xia, M.X. Ji, J. Di, B. Wang, S. Yin, M.Q. He, Q. Zhang, H.M. Li, Improved photocatalytic activity of few-layer  $\text{Bi}_4\text{O}_5\text{I}_2$  nanosheets induced by efficient charge separation and lower valence position, *J. Alloys Compd.* 695 (2017) 922–930.

[25] C.X. Zheng, G.P. He, X. Xiao, M.L. Lu, H. Zhong, X.X. Zuo, J.M. Nan, Selective photocatalytic oxidation of benzyl alcohol into benzaldehyde with high selectivity and conversion ratio over  $\text{Bi}_4\text{O}_5\text{Br}_2$  nanoflakes under blue LED irradiation, *Appl. Catal. B Environ.* 205 (2017) 201–210.

[26] G.J. Wu, Y. Zhao, Y.W. Li, H.M. Ma, J.Z. Zhao, pH-dependent synthesis of iodine-deficient bismuth oxyiodide microstructures: visible-light photocatalytic activity, *J. Colloid Interface Sci.* 510 (2018) 228–236.

[27] X. Xiao, R. Hao, X.X. Zuo, J.M. Nan, L.S. Lia, W.D. Zhang, Microwave-assisted synthesis of hierarchical  $\text{Bi}_7\text{O}_9\text{I}_3$  microsheets for efficient photocatalytic degradation of bisphenol A under visible light irradiation, *Chem. Eng. J.* 209 (2012) 293–300.

[28] X. Xiao, J. Jiang, L. Zhang, Selective oxidation of benzyl alcohol into benzaldehyde over semiconductors under visible light: the case of  $\text{Bi}_{12}\text{O}_{17}\text{C}_{12}$  nanobelts, *Appl. Catal. B* 142–143 (2013) 487–493.

[29] C.Y. Wang, X. Zhang, H.B. Qiu, W.K. Wang, G.X. Huang, J. Jiang, H.Q. Yu, Photocatalytic degradation of bisphenol A by oxygen-rich and highly visible-light responsive  $\text{Bi}_{12}\text{O}_{17}\text{C}_{12}$  nanobelts, *Appl. Catal. B* 200 (2017) 659–665.

[30] X. Jin, L. Ye, H. Wang, Y. Su, H. Xie, Z. Zhong, H. Zhang, Bismuth-rich strategy induced photocatalytic molecular oxygen activation properties of bismuth oxyhalogen: the case of  $\text{Bi}_{24}\text{O}_{31}\text{Cl}_{10}$ , *Appl. Catal. B* 165 (2015) 668–675.

[31] X. Xiao, R. Hu, C. Liu, C. Xing, X. Zuo, J. Nan, L. Wang, Facile microwave synthesis of novel hierarchical  $\text{Bi}_{24}\text{O}_{31}\text{Br}_{10}$  nanoflakes with excellent visible light photocatalytic performance for the degradation of tetracycline hydrochloride, *Chem. Eng. J.* 225 (2013) 790–797.

[32] J. Chen, M.L. Guan, W.Z. Cai, J.J. Guo, C. Xiao, G.K. Zhang, The dominant {001} facet-dependent enhanced visible-light photoactivity of ultrathin  $\text{BiOBr}$  nanosheets, *Phys. Chem. Chem. Phys.* 16 (2014) 20909–20914.

[33] Z. Wan, G.K. Zhang, X.Y. Wu, S. Yin, Novel visible-light-driven Z-scheme  $\text{Bi}_{12}\text{GeO}_{20}/\text{g-C}_3\text{N}_4$  photocatalyst: oxygen-induced pathway of organic pollutants degradation and proton assisted electron transfer mechanism of Cr(VI) reduction, *Appl. Catal. B Environ.* 207 (2017) 17–26.

[34] S.H. Tu, M.L. Lu, X. Xiao, C.X. Zheng, H. Zhong, X.X. Zuo, J.M. Nan, Flower-like  $\text{Bi}_4\text{O}_5\text{I}_2/\text{Bi}_5\text{O}_7\text{I}$  nanocomposite: facile hydrothermal synthesis and efficient photocatalytic degradation of propylparaben under visible-light irradiation, *RSC Adv.* 6 (2016) 44552–44560.

[35] Z. Wan, G.K. Zhang, Synthesis and facet-dependent enhanced photocatalytic activity of  $\text{Bi}_2\text{SiO}_5/\text{AgI}$  nanoplate photocatalysts, *J. Mater. Chem. A* 3 (2015) 16737–16745.

[36] J.J. Zheng, F. Chang, M.Z. Jiao, Q. Xu, B.Q. Deng, X.F. Hu, A visible-light-driven heterojuncted composite  $\text{WO}_3/\text{Bi}_{12}\text{O}_{17}\text{Cl}_2$ : synthesis, characterization, and improved photocatalytic performance, *J. Colloid Interface Sci.* 510 (2018) 20–31.

[37] H.W. Huang, K. Xiao, T.R. Zhang, F. Dong, Y.H. Zhang, Rational design on 3D hierarchical bismuth oxyiodides via *in situ* self-template phase transformation and phase-junction construction for optimizing photocatalysis against diverse contaminants, *Appl. Catal. B Environ.* 203 (2017) 879–888.

[38] Y. Bai, L.Q. Ye, L. Wang, X. Shi, P.Q. Wang, W. Bai, P.K. Wong,  $\text{g-C}_3\text{N}_4/\text{Bi}_4\text{O}_5\text{I}_2$  heterojunction with  $\text{I}_3^-/\text{I}^-$  redox mediator for enhanced photocatalytic  $\text{CO}_2$  conversion, *Appl. Catal. B Environ.* 194 (2016) 98–104.

[39] J. Di, J.X. Xia, Y.P. Ge, L. Xu, H. Xu, M.Q. He, Q. Zhang, H.M. Li, Reactable ionic liquid-assisted rapid synthesis of  $\text{BiOI}$  hollow nanospheres at room temperature with enhanced photocatalytic activity, *J. Mater. Chem. A* 2 (2014) 15864–15874.

[40] Q.C. Liu, D.K. Ma, Y.Y. Hu, Y.W. Zeng, S.M. Huang, Various bismuth oxyiodide hierarchical architectures: Alcoothermal-controlled synthesis, photocatalytic activities, and adsorption capabilities for phosphate in water, *ACS Appl. Mater. Interfaces* 5 (2013) 11927–11934.

[41] S.Y. Chou, C.C. Chen, Y.M. Dai, J.H. Lin, W.W. Lee, Novel synthesis of bismuth oxyiodide/graphitic carbon nitride nanocomposite with enhanced visible-light photocatalytic activity, *RSC Adv.* 6 (2016) 33478–33491.

[42] C. Liu, X.J. Wang, Room temperature synthesis of  $\text{Bi}_4\text{O}_5\text{I}_2$  and  $\text{Bi}_5\text{O}_7\text{I}$  ultrathin nanosheets with a high visible light photocatalytic performance, *Dalton Trans.* 45 (2016) 7720–7727.

[43] A. Chatzitakis, C. Berberidou, I. Paspaltsis, G. Kyriakou, T. Sklaviadis, I. Poulios, Photocatalytic degradation and drug activity reduction of Chloramphenicol, *Water Res.* 42 (2008) 386–394.

[44] H.W. Huang, Y. He, Z.S. Lin, L. Kang, Y.H. Zhang, Two novel Bi-based borate photocatalysts: crystal structure, electronic structure, photoelectrochemical properties, and photocatalytic activity under simulated solar light irradiation, *J. Phys. Chem. C* 117 (2013) 22986–22994.

[45] X.J. Bai, L. Wang, Y.F. Zhu, Visible photocatalytic activity enhancement of  $\text{ZnWO}_4$  by graphene hybridization, *ACS Catal.* 2 (2012) 2769–2778.

[46] L.H. Yu, X.Y. Zhang, G.W. Li, Y.T. Cao, Y. Shao, D.Z. Li, Highly efficient  $\text{Bi}_2\text{O}_2\text{CO}_3/\text{BiOCl}$  photocatalyst based on heterojunction with enhanced dye-sensitization under visible light, *Appl. Catal. B Environ.* 187 (2016) 301–309.

[47] Y.P. Luo, J. Chen, J.W. Liu, Y. Shao, X.F. Li, D.Z. Li, Hydroxide  $\text{SrSn}(\text{OH})_6$ : a new photocatalyst for degradation of benzene and rhodamine B, *Appl. Catal. B Environ.* 182 (2016) 533–540.

[48] Y.H. Ao, K.D. Wang, P.F. Wang, C. Wang, J. Hou, Synthesis of novel 2D-2D p-n heterojunction  $\text{BiOBr}/\text{La}_2\text{Ti}_2\text{O}_7$  composite photocatalyst with enhanced photocatalytic performance under both UV and visible light irradiation, *Appl. Catal. B Environ.* 194 (2016) 157–168.

[49] R.F. Dong, B.Z. Tian, C.Y. Zeng, T.Y. Li, T.T. Wang, J.L. Zhang, Ecofriendly synthesis and photocatalytic activity of uniform cubic  $\text{Ag}/\text{AgCl}$  plasmonic photocatalyst, *J. Phys. Chem. C* 117 (1) (2013) 213–220.

[50] M. Sun, Q. Zeng, X. Zhao, Y. Shao, P.G. Ji, C.Q. Wang, T. Yan, B. Du, Fabrication of novel  $\text{g-C}_3\text{N}_4$  nanocrystals decorated  $\text{Ag}_3\text{PO}_4$  hybrids: enhanced charge separation and excellent visible-light driven photocatalytic activity, *J. Hazard. Mater.* 339 (2017) 9–21.

[51] L.S. Zhang, K.H. Wong, D.Q. Zhang, C. Hu, J.C. Yu, C.Y. Chan, P.K. Wong, Zn:in  $(\text{OH})_2\text{S}_2$  solid solution nanoplates: synthesis, characterization, and photocatalytic mechanism, *Environ. Sci. Technol.* 43 (2009) 7883–7888.